ACS APPLIED MATERIALS & INTERFACES

www.acsami.org

Research Article

Electromagnetic-Polarization-Selective Composites with Quasi-1D Van der Waals Fillers: Nanoscale Material Functionality That Mimics Macroscopic Systems

Zahra Barani, Fariborz Kargar,* Yassamin Ghafouri, Saba Baraghani, Sriharsha Sudhindra, Amirmahdi Mohammadzadeh, Tina T. Salguero, and Alexander A. Balandin*

Cite This: *ACS Appl. Mater. Interfaces* 2021, 13, 21527−21533

Read Online

ACCESS | Metrics & More | Article Recommendations | Supporting Information

ABSTRACT: We report on the preparation of flexible polymer composite films with aligned metallic fillers composed of atomic chain bundles of quasi-one-dimensional (1D) van der Waals material, tantalum triselenide ($TaSe_3$). The material functionality, embedded at the nanoscale level, is achieved by mimicking the design of an electromagnetic aperture grid antenna. The processed composites employ chemically exfoliated $TaSe_3$ nanowires as the grid building blocks incorporated within the thin film. Filler alignment is achieved using the "blade coating" method. Measurements conducted in the X-band frequency range demonstrate that the electromagnetic transmission through such films can be varied significantly by changing the relative orientations of the quasi-1D fillers and the polarization of the electromagnetic wave. We argue that such polarization-sensitive polymer films with unique quasi-1D metallic fillers are applicable to advanced electromagnetic interference shielding in future communication systems.

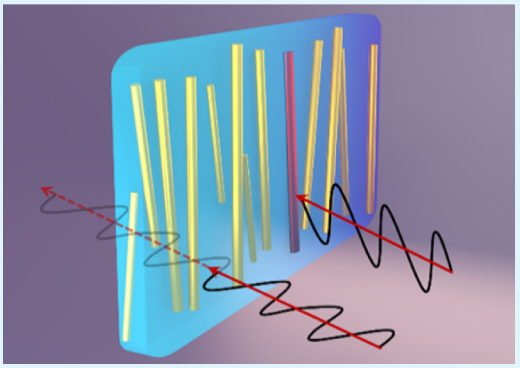

KEYWORDS: *quasi-1D van der Waals materials, polymer composites, electromagnetic properties, GHz frequency, EMI shielding*

INTRODUCTION

Commonly, one selects functional materials with known characteristics to build a device or a system. In more elaborate approaches, one can engineer and synthesize materials with the required properties for specific applications. The inspiration for material selection, composition, and assembly can come from diverse sources. In one well-known approach, biomimetics, the models and elements of nature are applied to the design of synthetic systems.[1,2] In an analogous approach, well-developed design solutions for macroscopic objects are translated into micro-, nano-, or atomic-scale structures. We followed this innovative path to create a polymer composite with polarization-sensitive electromagnetic interference (EMI) shielding characteristics by emulating the macroscopic structure and, to some degree, the functionality of an electromagnetic (EM) grid aperture antenna at the nanoscale level. A polarization-selective grid antenna is a set of parallel metal grid lines that allow transmission or reflection of radio-frequency (RF) radiation depending on the polarization of the radiation.[3] This design allows a single structure to act as a mirror for RF radiation or become transparent to such radiation. When the polarization of the electric field is parallel to the grid lines, the electric field induces a current in the grid lines, which reflects the EM wave. In the alternate case, with the polarization of the electric field perpendicular to the grid lines, no current is induced, and the EM radiation passes through the grid. Polarization selection grids are often manufactured with metal wire tracks, usually copper, on a dielectric substrate. The spacings between grid lines must be small relative to the wavelength of the linear polarized EM waves. Here, we use a similar antenna design, albeit at the nanometer scale, to create a "grid antenna film".

In this work, we mimic the grid antenna design in nanocomposites by employing chemically exfoliated bundles of a quasi-one-dimensional (1D) van der Waals material, tantalum triselenide ($TaSe_3$). We recently demonstrated the potential of $TaSe_3$ for extremely high current density[4−6] and effective EMI shielding, even with random filler distribution and low filler loading fractions.[7] Such quasi-1D van der Waals materials are less investigated compared with two-dimensional (2D) layered van der Waals materials, such as graphene and transition-metal dichalcogenides (TMDs).[8−10] The quasi-1D van der Waals materials include the transition-metal

Received: February 18, 2021
Accepted: April 20, 2021
Published: April 30, 2021

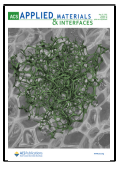

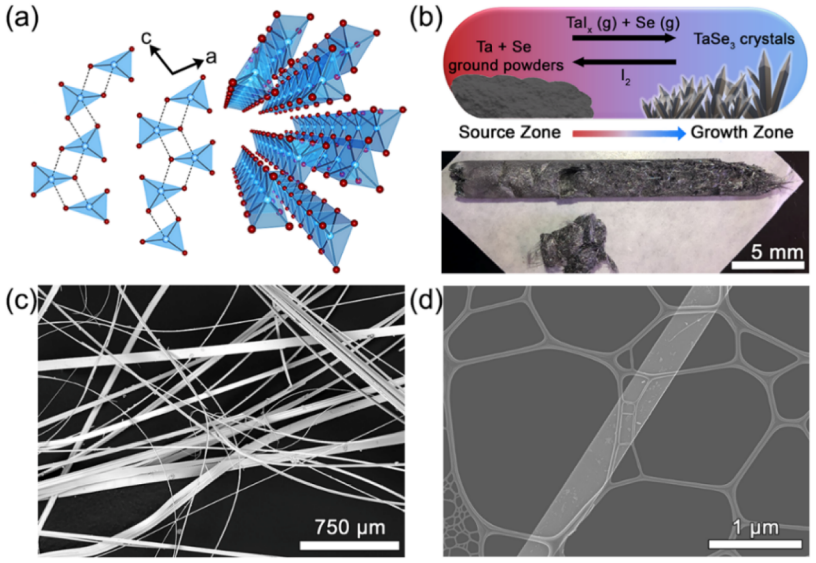

Figure 1. Crystal structure of quasi-1D $TaSe_3$ used in this study. (a) Crystal structure of $TaSe_3$ (blue, Ta; red, Se) with two views illustrating interchain interactions and emphasizing on material's 1D nature originating from chains extending along the *b*-axis. (b) Schematic of the chemical vapor transport (CVT) process employed here to prepare $TaSe_3$ crystals (top) and a photograph of an as-synthesized mass of crystals removed from its growth ampule (below). (c) Scanning electron microscopy (SEM) image of $TaSe_3$ crystals highlighting their high aspect ratio. (d) Secondary electron (SE) image of a $TaSe_3$ nanowire produced by solvent exfoliation.

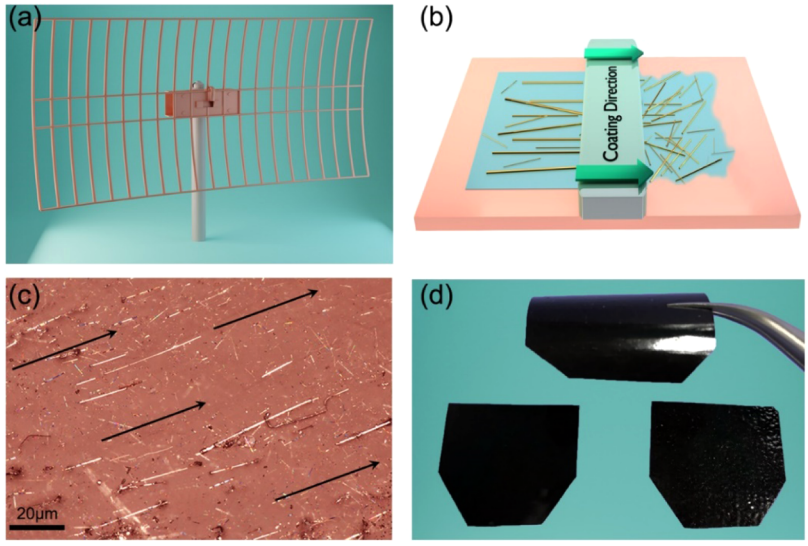

Figure 2. System-level concept and material-level implementation. (a) View of the aperture grid antenna illustrating the macroscopic model of the synthesized polymer nanocomposites with aligned quasi-1D fillers. (b) Schematic of the blade coating filler alignment process in the polymer films, in which the bundles of quasi-1D atomic threads function as metal wires in a grid antenna. (c) Optical microscopy image of the UV-cured polymer film with 1.8 vol % of $TaSe_3$ quasi-1D fillers. Note the aligned high-aspect-ratio $TaSe_3$ fillers along the coating direction. (d) Optical image of the resulting flexible polymer films with incorporated quasi-1D fillers, which mimic the action of a grid antenna.

trichalcogenides (TMTs) with formula MX_3 (M = transition metal, X = S, Se, Te), such as TiS_3, NbS_3, $TaSe_3$, and $ZrTe_3$, as well as other materials containing 1D structural motifs.[11−13] As opposed to TMDs, TMTs exfoliate into nanowire- or nanoribbon-type structures,[4,12−15] which stem from their unique chain-based crystal structures, illustrated for $TaSe_3$ in Figure 1a. In principle, these low-dimensional materials can be exfoliated into individual atomic chains or few-chain atomic threads. Theory suggests that there are many quasi-1D van der Waals materials that retain their metallic or semiconductor properties when exfoliated to atomic chains.[16−18] The exfoliated bundles of $TaSe_3$ atomic threads with cross sections in the range of 10 nm × 10 nm to 100 nm × 100 nm revealed exceptionally high current densities of up to ∼30 MA/cm^2, an order of magnitude higher than that of copper.[19,20] Additionally, the liquid-phase-exfoliated (LPE) $TaSe_3$ bundles can be millimeters in length, providing substantial aspect ratios. The unique current-carrying capability of the metallic $TaSe_3$, in addition to their high aspect ratios, allows us to use them as "metallic grids" even when scaled down to 100 nm features or below. The quasi-1D van der Waals metallic fillers can be mass-produced at low cost via liquid-phase exfoliation. This adds a significant extra benefit to such materials as compared to carbon nanotubes.

https://doi.org/10.1021/acsami.1c03204
ACS Appl. Mater. Interfaces 2021, 13, 21527−21533

EXPERIMENTAL SECTION

Materials. For this study, we used $TaSe_3$ crystals prepared by chemical vapor transport (CVT). In contrast to typical CVT reactions, where the goal is the growth of a relatively small number of larger crystals,[4,5,7,15] here we varied reaction conditions to yield 0.7−1.5 g batches of $TaSe_3$ crystals for composite preparation. Transport was achieved using iodine as the transport agent and/or using a 625−600 °C temperature gradient. As can be seen in Figure 1b, the scale of these reactions led to the growth of $TaSe_3$ crystals almost entirely filling the ampule volume. The resulting mat of crystals could be removed easily, providing 18−38% yields of mm- to cm-long needle-like or fibrous crystals (Figure 1b) and also leaving behind a quantity of microcrystalline solid that was not used for subsequent exfoliation. The long crystals have smooth faces and straight edges that characterize high-quality $TaSe_3$ samples (Figures 1c,d and S1). Powder X-ray diffraction (Figure S2) and energy-dispersive spectroscopy (see Table S1 for compositional analysis) provided analytical results consistent with the standard structure of $TaSe_3$, albeit with some variation in the Se content.

Composite Preparation and Characterization. These CVT-grown $TaSe_3$ crystals were subjected to the LPE following the process reported by us elsewhere.[7,21] Figure 2 summarizes our approach of mimicking the grid antenna design using material synthesis and presents optical images of the partially aligned fillers in the polymer composites and the resulting films. We used the "blade coating" method to prepare flexible thin films with a thickness of 100 ± 10 μm with a special type of UV-cured polymer and exfoliated $TaSe_3$ as fillers. In this method, a small amount of polymer−filler solution is drop-cast on a rigid substrate with a smooth surface.[22−24] A blade with an adjustable distance from the top surface of the substrate is gradually run over the mixture, and the compound is spread over the substrate (Figure 2b). Using this technique, the quasi-1D fillers are aligned, to some extent, in the direction of the coating owing to the applied viscoelastic shear stress as a result of blade movement[22,23] (Figure 2c). The samples are referred to as A, B, C, and D throughout this manuscript with filler concentrations of 2.2, 1.03, 1.87, and 1.61 vol %, respectively. The properties of the samples are summarized in Table S2 of the Supporting Information.

EM Shielding Measurements. We conducted EM testing of the prepared films in the X-band frequency range (f = 8.2−12.4 GHz), which is pertinent to the current and future communication technologies. To determine the polarization selectivity, we followed the measurement protocols used in the EMI shielding testing.[25−30] We measured the scattering parameters, S_{ij}, with the two-port programmable network analyzer (PNA; Keysight N5221A). The measured scattering parameters are related to the coefficients of reflection, $R = |S_{11}|^2$, and transmission, $T = |S_{21}|^2$. The measurements were carried out in a WR-90 commercial-grade straight waveguide with two adapters at both ends with SMA coaxial ports. The samples were made a bit larger than the rectangular cross section (a = 22.8 mm, b = 10.1 mm) of the central hollow part of the waveguide to prevent the leakage of the EM waves from the sender to the receiver antenna. The cutoff frequency for different fundamental transverse electric (TE) modes in .rectangular-shaped waveguides is given by the formula $(f_c)_{mn} = \frac{1}{2\pi\sqrt{\mu\varepsilon}}\sqrt{(m\pi/a)^2 + (n\pi/b)^2}$ [Hz], where m and n are the positive integer numbers.[31] Therefore, the dominant EM mode in WR-90 waveguide is the TE_{10} mode with electrical field (E) oscillating in the vertical direction perpendicular to the larger side of the inlet aperture (see Figure 3). The frequencies of other modes exceed the X-band frequency range and are not of interest in this study.

RESULTS AND DISCUSSION

To investigate the effect of the filler alignment on the EM characteristics of the composites, measurements were carried out at different sample orientation angles (α) by rotating the sample about the guide axis. Note that α is the angle between the aligned filler chains in the composite with respect to the larger side of the guide's aperture. Therefore, at α = 0°, the fillers are parallel to the larger side and E is perpendicular to them. The front-view schematic of the WR-90 waveguide, the electric field configuration of the TE_{10} mode, and its mutual orientation with respect to the quasi-1D fillers of the composites are shown in Figure 3. Figure 4 presents the reflection (SE_R), absorption (SE_A), and total (SE_T) shielding effectiveness of samples A and C with 2.2 and 1.87 vol % filler concentrations, respectively, as a function of EM frequency when the polarization of the incident EM wave is either parallel with (∥) or transverse to (⊥) the quasi-1D fillers. Note that the shielding effectiveness of the films is significantly enhanced when E is parallel to the filler alignment compared to that perpendicular to the filler chains. For samples A and C, the enhancement in the total shielding effectiveness, defined as $\eta = (SE_{T,\parallel} - SE_{T,\perp})/SE_{T,\perp}$, is 128% and 107%, respectively (see Table S2 for more details).

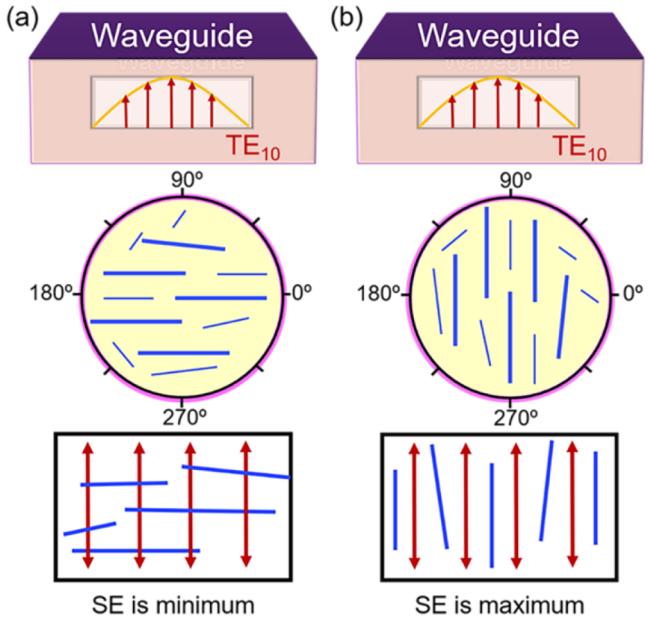

Figure 3. Experimental procedures. Front-view schematic of the standard WR-90 waveguide, and polarization of the allowed fundamental TE_{10} mode propagating in this type of waveguide at a given frequency range. (a) At α = 0°, the bundles of the quasi-1D atomic chains are parallel to the larger side of the aperture and perpendicular to the electric field of the TE_{10} mode. (b) At α = 90°, the bundles are perpendicular to the larger side of the aperture and thus parallel to the electric field of the TE_{10} mode.

We measured the angular dependence of SE_T of all four samples at a constant frequency of f = 8.2 GHz to elucidate the effect of the filler alignment on EM shielding properties of the composites. The results of these measurements are presented in Figure 5. Note that at α = 0°, E is perpendicular to the filler atomic chains. One can notice the sinusoidal characteristic of the SE_T (solid lines) with a period of 180° as a function of α. When the fillers are aligned in one direction, the composite film becomes anisotropic, given that the embedding matrix is isotropic. This behavior is consistent for all examined samples with different loadings of the aligned quasi-1D fillers. If the fillers were randomly distributed inside the polymers, one would expect isotropic EMI shielding properties, i.e., with rotating the sample, EMI properties would remain almost the same. In fact, the shielding effectiveness of the samples prepared by the "compressional molding", with randomly

https://doi.org/10.1021/acsami.1c03204
ACS Appl. Mater. Interfaces 2021, 13, 21527−21533

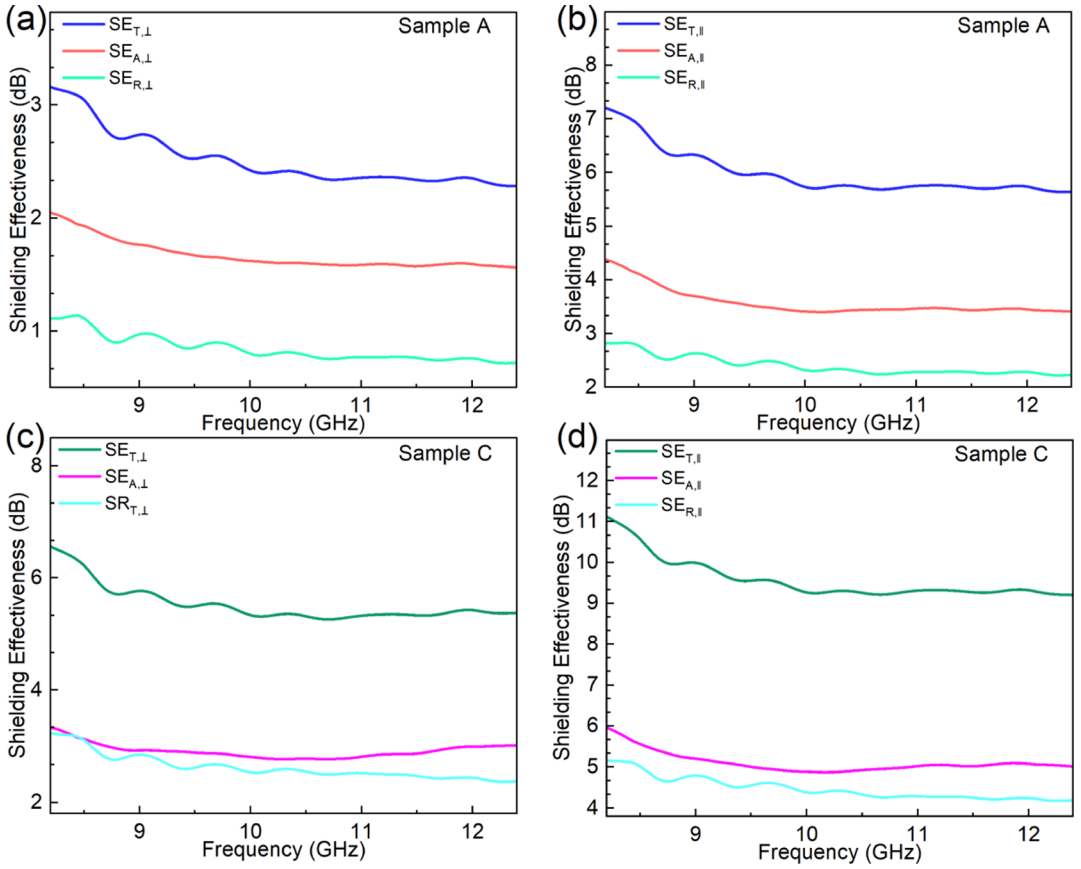

Figure 4. Electromagnetic data. Reflection (SE_R), absorption (SE_A), and total (SE_T) EMI shielding effectiveness of (a, b) sample A and (c, d) sample C for two cases of the EM wave polarization transverse to (⊥) and parallel with (∥) the quasi-1D fillers. Note that EMI shielding is significantly higher when the polarization is parallel to the filler alignment.

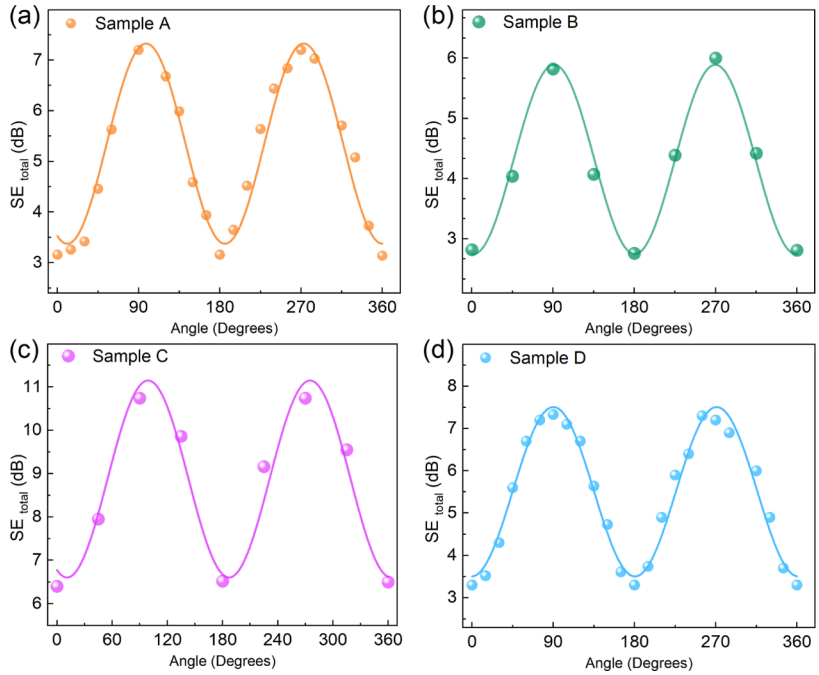

Figure 5. Electromagnetic-polarization-selective composites. Total shielding effectiveness of samples with filler contents of (a) 2.2 vol %, (b) 1.03 vol %, (c) 1.87 vol %, and (d) 1.61 vol % as a function of the composite orientation angle α, measured at 8.2 GHz frequency. At $\alpha = 0°$, the polarization of the EM wave is perpendicular to the filler alignment. The results are fitted with sine functions. Note the periodicity of the SE_T with a period of 180°.

https://doi.org/10.1021/acsami.1c03204
ACS Appl. Mater. Interfaces 2021, 13, 21527−21533

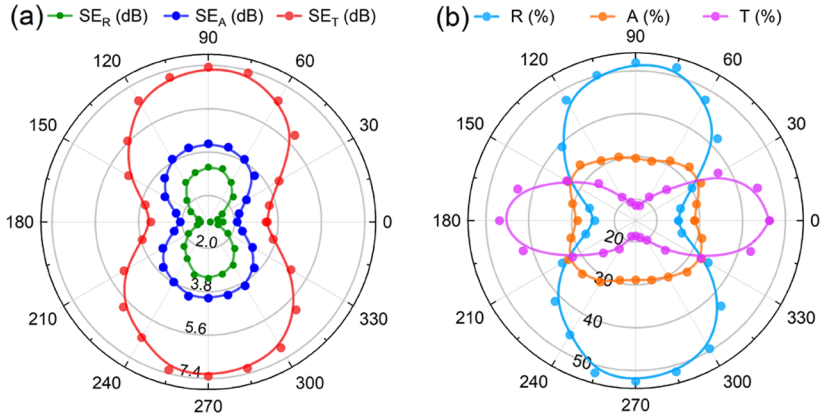

Figure 6. Contribution of different mechanisms to interaction with EM waves. The angular dependency of (a) the reflection, absorption, and total shielding effectiveness and (b) reflection absorption and transmission coefficients of sample D with 1.61 vol % aligned quasi-1D $TaSe_3$ fillers. Note the extremes at 0 and 90° and the symmetry of the curves in both panels confirming the alignment of fillers inside the polymer matrix. As shown in (b), the reflection is highly correlated with the sample orientation, whereas absorption varies weakly.

oriented fillers, does not exhibit any angular dependency characteristic (see the Supporting Information, Figures S8 and S9). The latter provides additional evidence of the filler alignment when the blade coating method is applied during the sample synthesis.

The periodic EM shielding characteristics observed in our composites originate from two different effects: (i) the prolate ellipsoidic needle-like geometry of the fillers, assuming semi-axes of $a_x > a_y = a_z$, and (ii) the anisotropic complex permittivity properties of the quasi-1D $TaSe_3$ fillers.[32] Because the filler inclusion is low in all of the samples, the Maxwell–Garnett (M–G) effective medium theory can be used to explain the observed characteristics.[32,33] For composites with aligned dielectric fillers, the M–G effective complex permittivity of the composite along the x direction, $\varepsilon_{c,x}$, can be described as

$$\varepsilon_{c,x} = \varepsilon_p + \phi_f \varepsilon_p \frac{\varepsilon_f - \varepsilon_p}{\varepsilon_f + (1 - \phi_f) N_x (\varepsilon_f - \varepsilon_p)} \quad (1)$$

In this equation, ε_p and ε_f are the permittivity of the polymer and filler, respectively, and ϕ_f is the filler volume fraction. For ellipsoidal fillers, the depolarization factor is given as $N_x = \left(\frac{1-e^2}{2e^3}\right)\left(\ln\frac{1+e}{1-e} - 2e\right)$, where $e = \sqrt{1 - a_y^2/a_x^2}$ is eccentricity.[32] Considering the large aspect ratio of the exfoliated fillers ($a_x \gg a_y$), it can be easily inferred that the effective permittivity of the composites would be largely different along different directions, i.e., parallel with and perpendicular to the aligned atomic chains. Note that to obtain the effective permittivity along other directions, y and z, the depolarization factor should be replaced by N_y and N_z and calculated accordingly.

The special geometrical shape of the aligned fillers is not the only parameter causing anisotropic behavior of composites with quasi-1D fillers. Owing to the monoclinic crystal structure of $TaSe_3$, the EM properties of the fillers are highly directional. The polarized reflectance data of $TaSe_3$ exhibits metallic characteristics in the infrared region.[34] To the best of our knowledge, there are no data on the dielectric properties of $TaSe_3$ in the microwave region. However, one can describe the complex dielectric parameter of $TaSe_3$ as a function of the EM frequency, ω, by the Lorentz–Drude model, $\varepsilon(\omega) = \varepsilon_\infty - \frac{\omega_p^2}{\omega^2 - i\omega\Gamma_0} + \sum_m^{n=1} \frac{\omega_{p,n}^2}{\omega_{0,n}^2 - \omega^2 - i\omega\Gamma_n}$.[34] In this model, ε_∞ is the permittivity of the material when the frequency goes to infinity and m is the number of the oscillators with the frequency of $\omega_{0,n}$ and the lifetime of $1/\Gamma_n$. The plasma frequency, $\omega_p = \sqrt{Nq^2/m^*\varepsilon_0}$, depends on the electron density, N, electron absolute charge, q, and the effective mass of electrons, m^*. The second and third terms are associated with the interaction of EM waves with the intraband, or free electrons, and interband, or bound electrons, respectively. The $\hbar\omega_p$ in $TaSe_3$ along the crystallographic "a" (perpendicular to the chains) and "b" (along the chains) axes are 0.42 and 0.68 eV.[34] Therefore, one would expect an anisotropic frequency-dependent reflectance (R) and conductance (σ) along with and perpendicular to the atomic chains in the microwave region, with both parameters being larger in the direction along the atomic chains. Such strong, anisotropic reflectance properties have been reported for $TaSe_3$ in the EM energy range between 0.05 and 5 eV, previously.[35]

Figure 6a,b exhibits the angular-dependent reflection, absorption, and transmission shielding effectiveness and coefficients of sample D, respectively. The fourfold symmetry of all plots shown in both panels confirms the alignment of quasi-1D fillers. More importantly, as seen in Figure 6b, reflection is the dominant mechanism of shielding of the EM waves in the microwave region. The reflection coefficient increases more than two times compared to the two extreme cases of $\alpha = 0$ and 90°, whereas the absorption almost does not vary. The fourfold symmetric transmission curve in Figure 6b demonstrates the applicability of prepared flexible films as microwave attenuators or grid polarizers. For reference, the shielding effectiveness in the samples prepared by the compressional molding does not reveal any angular dependence (see the Supporting Information, Figures S7a and S8). The observed EM property is similar to the linear dichroism, which has been reported in the visible light region for bulk and exfoliated MPX_3 crystals with strong optical anisotropy.[36,37] Bulk TiS_3 exhibits a linear dichroism with a transmittance ratio of $\zeta = T_\perp/T_\parallel = 30$ at a wavelength of 633 nm.[38]

https://doi.org/10.1021/acsami.1c03204
ACS Appl. Mater. Interfaces 2021, 13, 21527–21533

CONCLUSIONS

In conclusion, we have described the preparation and properties of flexible polymer composite films with aligned metallic fillers made of bundles of quasi-one-dimensional (1D) van der Waals metal, characterized by high current density. The material functionality, embedded at the nanoscale level, was achieved by mimicking the design of an electromagnetic aperture grid antenna. The synthesized composites use the quasi-1D van der Waals nanowires as the grid building block incorporated within the thin film structure. The measurements conducted in the X-band frequency range demonstrated that the electromagnetic transmission through such films could be varied by changing the mutual orientation of the quasi-1D fillers and polarization of the electromagnetic wave. The films with a low loading of the quasi-1D fillers (<2 vol %) and only partial alignment of the fillers can already produce a ∼5 dB variation in the transmitted signal. We argue that such polarization-sensitive polymer films with quasi-1D fillers can be used for advanced electromagnetic interference shielding in future communication systems.

ASSOCIATED CONTENT

Supporting Information

The Supporting Information is available free of charge at https://pubs.acs.org/doi/10.1021/acsami.1c03204.

Detailed description of the $TaSe_3$ growth and synthesis and its SEM, XRD, EDS characterizations, composite preparation and characterization, electromagnetic measurement technique, as well as additional data on shielding effectiveness of the base polymer and films prepared by other methods (PDF)

AUTHOR INFORMATION

Corresponding Authors

Fariborz Kargar − *Nano-Device Laboratory (NDL) and Phonon Optimized Engineered Materials (POEM) Center, Department of Electrical and Computer Engineering, University of California, Riverside, California 92521, United States; Department of Chemical and Environmental Engineering, University of California, Riverside, California 92521, United States;* orcid.org/0000-0003-2192-2023; Email: fkargar@ece.ucr.edu

Alexander A. Balandin − *Nano-Device Laboratory (NDL) and Phonon Optimized Engineered Materials (POEM) Center, Department of Electrical and Computer Engineering, University of California, Riverside, California 92521, United States; Material Science and Engineering Program, University of California, Riverside, California 92521, United States;* Email: balandin@ece.ucr.edu

Authors

Zahra Barani − *Nano-Device Laboratory (NDL) and Phonon Optimized Engineered Materials (POEM) Center, Department of Electrical and Computer Engineering, University of California, Riverside, California 92521, United States*

Yassamin Ghafouri − *Department of Chemistry, University of Georgia, Athens, Georgia 30602, United States*

Saba Baraghani − *Nano-Device Laboratory (NDL) and Phonon Optimized Engineered Materials (POEM) Center, Department of Electrical and Computer Engineering, University of California, Riverside, California 92521, United States; Department of Chemical and Environmental Engineering, University of California, Riverside, California 92521, United States*

Sriharsha Sudhindra − *Nano-Device Laboratory (NDL) and Phonon Optimized Engineered Materials (POEM) Center, Department of Electrical and Computer Engineering, University of California, Riverside, California 92521, United States*

Amirmahdi Mohammadzadeh − *Nano-Device Laboratory (NDL) and Phonon Optimized Engineered Materials (POEM) Center, Department of Electrical and Computer Engineering, University of California, Riverside, California 92521, United States*

Tina T. Salguero − *Department of Chemistry, University of Georgia, Athens, Georgia 30602, United States;* orcid.org/0000-0001-9396-3583

Complete contact information is available at: https://pubs.acs.org/10.1021/acsami.1c03204

Author Contributions

A.A.B. and F.K. conceived the idea of the EMI shielding films with oriented quasi-1D van der Waals fillers, planned the study, and led the manuscript preparation. Z.B. developed the testing protocols, prepared the composites, measured the EM characteristics, and contributed to data analysis. Y.G. synthesized bulk crystals and performed bulk crystal material characterization. S.S. performed LPE of the bulk crystals. S.B. assisted with the EM measurements and sample characterizations. A.M. conducted SEM characterization. T.T.S. supervised material synthesis and contributed to data analysis. All authors contributed to the writing and editing of the manuscript.

Notes

The authors declare no competing financial interest.

ACKNOWLEDGMENTS

The work at UC Riverside was supported, in part, by the National Science Foundation (NSF) program Designing Materials to Revolutionize and Engineer our Future (DMREF) via a project DMR-1921958 entitled Collaborative Research: Data Driven Discovery of Synthesis Pathways and Distinguishing Electronic Phenomena of 1D van der Waals Bonded Solids.

REFERENCES

(1) Parker, A. R.; Townley, H. E. Biomimetics of Photonic Nanostructures. *Nat. Nanotechnol.* **2007**, *2*, 347−353.

(2) Li, Y.; John, J.; Kolewe, K. W.; Schiffman, J. D.; Carter, K. R. Scaling Up Nature: Large Area Flexible Biomimetic Surfaces. *ACS Appl. Mater. Interfaces* **2015**, *7*, 23439−23444.

(3) Milligan, T. A. *Modern Antenna Design*; John Wiley & Sons, 2005.

(4) Stolyarov, M. A.; Liu, G.; Bloodgood, M. A.; Aytan, E.; Jiang, C.; Samnakay, R.; Salguero, T. T.; Nika, D. L.; Rumyantsev, S. L.; Shur, M. S.; Bozhilov, K. N.; Balandin, A. A. Breakdown Current Density in *h*-BN-Capped Quasi-1D $TaSe_3$ Metallic Nanowires: Prospects of Interconnect Applications. *Nanoscale* **2016**, *8*, 15774−15782.

(5) Liu, G.; Rumyantsev, S.; Bloodgood, M. A.; Salguero, T. T.; Shur, M.; Balandin, A. A. Low-Frequency Electronic Noise in Quasi-1D $TaSe_3$ van Der Waals Nanowires. *Nano Lett.* **2017**, *17*, 377−383.

(6) Empante, T. A.; Martinez, A.; Wurch, M.; Zhu, Y.; Geremew, A. K.; Yamaguchi, K.; Isarraraz, M.; Rumyantsev, S.; Reed, E. J.; Balandin, A. A.; Bartels, L. Low Resistivity and High Breakdown

Current Density of 10 nm Diameter van der Waals $TaSe_3$ Nanowires by Chemical Vapor Deposition. *Nano Lett.* **2019**, *19*, 4355−4361.
(7) Barani, Z.; Kargar, F.; Ghafouri, Y.; Ghosh, S.; Godziszewski, K.; Baraghani, S.; Yashchyshyn, Y.; Cywiński, G.; Rumyantsev, S.; Salguero, T. T.; Balandin, A. A. Electrically Insulating Flexible Films with Quasi-1D van der Waals Fillers as Efficient Electromagnetic Shields in the GHz and Sub-THz Frequency Bands. *Adv. Mater.* **2021**, *33*, No. 2007286.
(8) Novoselov, K. S.; Mishchenko, A.; Carvalho, A.; Castro Neto, A. H. 2D Materials and van der Waals Heterostructures. *Science* **2016**, *353*, No. aac9439.
(9) Geim, A. K.; Grigorieva, I. V. van der Waals Heterostructures. *Nature* **2013**, *499*, 419−425.
(10) Balandin, A. A. Thermal Properties of Graphene and Nanostructured Carbon Materials. *Nat. Mater.* **2011**, *10*, 569−581.
(11) Island, J. O.; Molina-Mendoza, A. J.; Barawi, M.; Biele, R.; Flores, E.; Clamagirand, J. M.; Ares, J. R.; Sánchez, C.; van der Zant, H. S. J.; D'Agosta, R.; Ferrer, I. J.; Castellanos-Gomez, A. Electronics and Optoelectronics of Quasi-1D Layered Transition Metal Trichalcogenides. *2D Mater.* **2017**, No. 022003.
(12) Patra, A.; Rout, C. S. Anisotropic Quasi-One-Dimensional Layered Transition-Metal Trichalcogenides: Synthesis, Properties and Applications. *RSC Adv.* **2020**, *10*, 36413−36438.
(13) Dai, J.; Li, M.; Zeng, X. C. Group IVB Transition Metal Trichalcogenides: A New Class of 2D Layered Materials beyond Graphene. *Wiley Interdiscip. Rev.: Comput. Mol. Sci.* **2016**, *6*, 211−222.
(14) Lipatov, A.; Loes, M. J.; Lu, H.; Dai, J.; Patoka, P.; Vorobeva, N. S.; Muratov, D. S.; Ulrich, G.; Kästner, B.; Hoehl, A.; Ulm, G.; Zeng, X. C.; Rühl, E.; Gruverman, A.; Dowben, P. A.; Sinitskii, A. Quasi-1D TiS_3 Nanoribbons: Mechanical Exfoliation and Thickness-Dependent Raman Spectroscopy. *ACS Nano* **2018**, *12*, 12713−12720.
(15) Geremew, A. K.; Rumyantsev, S.; Bloodgood, M. A.; Salguero, T. T.; Balandin, A. A. Unique Features of the Generation−Recombination Noise in Quasi-One-Dimensional van der Waals Nanoribbons. *Nanoscale* **2018**, *10*, 19749−19756.
(16) Cheon, G.; Duerloo, K.-A. N.; Sendek, A. D.; Porter, C.; Chen, Y.; Reed, E. J. Data Mining for New Two- and One-Dimensional Weakly Bonded Solids and Lattice-Commensurate Heterostructures. *Nano Lett.* **2017**, *17*, 1915−1923.
(17) Cheon, G.; Cubuk, E. D.; Antoniuk, E. R.; Blumberg, L.; Goldberger, J. E.; Reed, E. J. Revealing the Spectrum of Unknown Layered Materials with Superhuman Predictive Abilities. *J. Phys. Chem. Lett.* **2018**, *9*, 6967−6972.
(18) Saeed, Y.; Kachmar, A.; Carignano, M. A. First-Principles Study of the Transport Properties in Bulk and Monolayer MX_3 (M = Ti, Zr, Hf and X = S, Se) Compounds. *J. Phys. Chem. C* **2017**, *121*, 1399−1403.
(19) Lienig, J. In *Electromigration and Its Impact on Physical Design in Future Technologies*, Proceedings of the International Symposium on Physical Design, 2013; pp 33−40.
(20) Gambino, J. P.; Lee, T. C.; Chen, F.; Sullivan, T. D. In *Reliability Challenges for Advanced Copper Interconnects: Electromigration and Time-Dependent Dielectric Breakdown (TDDB)*, Proceedings of the International Symposium on the Physical and Failure Analysis of Integrated Circuits, IPFA, APS, 2009; pp 677−684.
(21) Nicolosi, V.; Chhowalla, M.; Kanatzidis, M. G.; Strano, M. S.; Coleman, J. N. Liquid Exfoliation of Layered Materials. *Science* **2013**, *340*, 1226419−1226419.
(22) Doganay, D.; Coskun, S.; Kaynak, C.; Unalan, H. E. Electrical, Mechanical and Thermal Properties of Aligned Silver Nanowire/Polylactide Nanocomposite Films. *Composites, Part B* **2016**, *99*, 288−296.
(23) Hu, T.; Song, Y.; Di, J.; Xie, D.; Teng, C. Highly Thermally Conductive Layered Polymer Composite from Solvent-Exfoliated Pristine Graphene. *Carbon* **2018**, *140*, 596−602.
(24) Kim, K.; Hong, J.; Hahm, S. G.; Rho, Y.; An, T. K.; Kim, S. H.; Park, C. E. Facile and Microcontrolled Blade Coating of Organic Semiconductor Blends for Uniaxial Crystal Alignment and Reliable Flexible Organic Field-Effect Transistors. *ACS Appl. Mater. Interfaces* **2019**, *11*, 13481−13490.
(25) Baker-Jarvis, J.; Janezic, M. D.; Degroot, D. C. High-Frequency Dielectric Measurements. *IEEE Instrum. Meas. Mag.* **2010**, *13*, 24−31.
(26) Kargar, F.; Barani, Z.; Balinskiy, M.; Magana, A. S.; Lewis, J. S.; Balandin, A. A. Dual-Functional Graphene Composites for Electromagnetic Shielding and Thermal Management. *Adv. Electron. Mater.* **2019**, *5*, No. 1800558.
(27) Barani, Z.; Kargar, F.; Mohammadzadeh, A.; Naghibi, S.; Lo, C.; Rivera, B.; Balandin, A. A. Multifunctional Graphene Composites for Electromagnetic Shielding and Thermal Management at Elevated Temperatures. *Adv. Electron. Mater.* **2020**, *6*, No. 2000520.
(28) Barani, Z.; Kargar, F.; Godziszewski, K.; Rehman, A.; Yashchyshyn, Y.; Rumyantsev, S.; Cywiński, G.; Knap, W.; Balandin, A. A. Graphene Epoxy-Based Composites as Efficient Electromagnetic Absorbers in the Extremely High-Frequency Band. *ACS Appl. Mater. Interfaces* **2020**, *12*, 28635−28644.
(29) Wei, Q.; Pei, S.; Qian, X.; Liu, H.; Liu, Z.; Zhang, W.; Zhou, T.; Zhang, Z.; Zhang, X.; Cheng, H.; Ren, W. Superhigh Electromagnetic Interference Shielding of Ultrathin Aligned Pristine Graphene Nanosheets Film. *Adv. Mater.* **2020**, *32*, No. 1907411.
(30) Li, X.-H.; Li, X.; Liao, K.-N.; Min, P.; Liu, T.; Dasari, A.; Yu, Z.-Z. Thermally Annealed Anisotropic Graphene Aerogels and Their Electrically Conductive Epoxy Composites with Excellent Electromagnetic Interference Shielding Efficiencies. *ACS Appl. Mater. Interfaces* **2016**, *8*, 33230−33239.
(31) Sadiku, M. N. O. *Elements of Electromagnetics*, 3rd ed.; Oxford University Press: New York, Oxford, 2005.
(32) Sihvola, A. Mixing Rules with Complex Dielectric Coefficients. *Subsurf. Sens. Technol. Appl.* **2000**, *1*, 393−415.
(33) Garnett, J. C. M. X. I. I. Colours in Metal Glasses and in Metallic Films. *Philos. Trans. R. Soc., A* **1904**, *203*, 385−420.
(34) Geserich, H. P.; Scheiber, G.; Lévy, F.; Monceau, P. Electrical Anisotropy of the Chain-like Conductors $NbSe_3$ and TaS_{e3}. *Physica B +C* **1986**, *143*, 174−176.
(35) Perucchi, A.; Søndergaard, C.; Mitrovic, S.; Grioni, M.; Barisic, N.; Berger, H.; Forró, L.; Degiorg, L. Spectroscopic and dc-Transport Investigations of the Electronic Properties of $TaSe_3$. *Eur. Phys. J. B* **2004**, *39*, 433−440.
(36) Papadopoulos, N.; Frisenda, R.; Biele, R.; Flores, E.; Ares, J. R.; Sánchez, C.; van der Zant, H. S. J.; Ferrer, I. J.; D'Agosta, R.; Castellanos-Gomez, A. Large Birefringence and Linear Dichroism in TiS_3 Nanosheets. *Nanoscale* **2018**, *10*, 12424−12429.
(37) Gilbert, S. J.; Yi, H.; Chen, J. S.; Yost, A. J.; Dhingra, A.; Abourahma, J.; Lipatov, A.; Avila, J.; Komesu, T.; Sinitskii, A.; Asensio, M. C.; Dowben, P. A. Effect of Band Symmetry on Photocurrent Production in Quasi-One-Dimensional Transition-Metal Trichalcogenides. *ACS Appl. Mater. Interfaces* **2020**, *12*, 40525−40531.
(38) Island, J. O.; Biele, R.; Barawi, M.; Clamagirand, J. M.; Ares, J. R.; Sánchez, C.; van der Zant, H. S. J.; Ferrer, I. J.; D'Agosta, R.; Castellanos-Gomez, A. Titanium Trisulfide (TiS_3): A 2D Semiconductor with Quasi-1D Optical and Electronic Properties. *Sci. Rep.* **2016**, *6*, No. 22214.

https://doi.org/10.1021/acsami.1c03204
ACS Appl. Mater. Interfaces 2021, 13, 21527−21533